
VARA-TTS: Non-Autoregressive Text-to-Speech Synthesis based on Very Deep VAE with Residual Attention

Peng Liu¹ Yuewen Cao^{*2} Songxiang Liu^{*2} Na Hu¹ Guangzhi Li¹ Chao Weng¹ Dan Su¹

Abstract

This paper proposes VARA-TTS¹, a non-autoregressive (non-AR) end-to-end text-to-speech (TTS) model using a very deep Variational Autoencoder (VDVAE) with Residual Attention mechanism, which refines the textual-to-acoustic alignment layer-wisely. Hierarchical latent variables with different temporal resolutions from the VDVAE are used as queries for the residual attention module. By leveraging the coarse global alignment from previous attention layer as an extra input, the following attention layer can produce a refined version of alignment. This amortizes the burden of learning the textual-to-acoustic alignment among multiple attention layers and outperforms the use of only a single attention layer in robustness. An utterance-level speaking speed factor is computed by a jointly-trained speaking speed predictor, which takes the mean-pooled latent variables of the coarsest layer as input, to determine number of acoustic frames at inference. Experimental results show that VARA-TTS achieves slightly inferior speech quality to an AR counterpart Tacotron 2 but an order-of-magnitude speed-up at inference; and outperforms an analogous non-AR model, BVAE-TTS, in terms of speech quality.

generate acoustic feature (e.g., mel-spectrogram) autoregressively from text input using an attention mechanism, and then synthesize audio samples from the acoustic feature with a neural vocoder (Oord et al., 2016; Kalchbrenner et al., 2018). However, the autoregressive (AR) structure has two major limitations: (1) it greatly limits the inference speed, since the inference time of AR models grows linearly with the output length; (2) the AR models usually suffer from robustness issues, e.g., word skipping and repeating, due to accumulated prediction error.

To avoid the aforementioned limitations of the AR TTS models, researchers have proposed various non-autoregressive (non-AR) TTS models (Ren et al., 2019; Peng et al., 2020; Ren et al., 2020; Kim et al., 2020; Miao et al., 2020; Lee et al., 2021). These models can synthesize acoustic features with significantly faster speed than AR models and reduce robustness issues, while achieving comparable speech quality to their AR counterparts. However, these models usually contain a separate duration module that does not propagate information to the acoustic module, which may lead to the training-inference mismatch issue. Moreover, the duration module needs duration labels as supervision, which may come from pre-trained AR TTS models (Ren et al., 2019; Peng et al., 2020), forced aligner (Ren et al., 2020), dynamic programming backtrack path (Kim et al., 2020) or jointly-trained attention modules (Miao et al., 2020; Lee et al., 2021).

In attention-based encoder-decoder TTS models, the keys and values are calculated from text, while the queries are differently constructed in various models. For AR TTS models like Tacotron (Wang et al., 2017), the queries are constructed from the AR hidden states. It is a natural choice since the AR hidden states contain the acoustic information up to the current frame. For non-AR TTS models like FLOW-TTS (Miao et al., 2020), only position information is used as query. For BVAE-TTS, the query is constructed from VAE latent variables. If the correlation between the queries and keys are not strong enough, it is difficult for attention module to learn the alignment between queries and keys. Therefore, the key to build a non-AR TTS model is constructing the queries that are highly correlated to keys and also enable parallel attention calculation.

1. Introduction

In recent years, text-to-speech (TTS) synthesis technologies have made rapid progress with deep learning techniques. Previous attention-based encoder-decoder TTS models have achieved state-of-the-art results in speech quality and intelligibility (Wang et al., 2017; Shen et al., 2018; Gibiansky et al., 2017; Ping et al., 2018b; Li et al., 2019). They first

^{*}Work done during internship at Tencent AI Lab. ¹Tencent AI Lab ²Human-Computer Communications Laboratory, The Chinese University of Hong Kong. Correspondence to: Peng Liu <laupeng1989@gmail.com>.

¹Codes will be released soon.

The corresponding text transcription can be considered as a lossy compression of the acoustic features. Meanwhile, the latent variables from hierarchical variational autoencoder (VAE) are also lossy compressions of acoustic features when trained on acoustic data. These latent variables may be correlated with the text and suitable to construct the queries. Moreover, hierarchical VAE provides latent variables of different resolutions, which can be used as the queries to build a coarse-to-fine layer-wise refined residual attention module. Specifically, the attention layer can use the alignment produced by the previous layer as an extra input and produce a refined version of the alignment. In this way, the burden of predicting the textual-to-acoustic alignment could be reduced and amortized by the coarse-to-fine attention layers. For the first attention layer, we can use a “nearly diagonal” initial alignment as a good instructive bias, considering the monotonic properties of text and acoustic features.

In this work, we present a novel non-AR TTS model based on a specific hierarchical VAE model called Very Deep VAE (VDVAE) and a coarse-to-fine layer-wise refined residual attention module. Our main contributions are as follows:

- We adopt VDVAE to model mel-spectrograms with bottom-up and top-down paths. The hierarchical latent variables serve as queries to the attention modules.
- We propose a novel residual attention mechanism that learns layer-wise alignments from coarse granularity to fine granularity in the top-down paths.
- We propose detailed Kullback-Leibler (KL) gain for VDVAE to avoid posterior collapse in some hierarchical layers.
- The proposed model is fully parallel and trained in an end-to-end manner, while obtaining high speech quality. Inference speed of the proposed model is 16 times faster than the AR model, Tacotron2, on a single NVIDIA GeForce RTX 2080 Ti GPU. Also, our proposed model outperforms an analogous non-AR model, BVAE-TTS, in terms of speech quality.

The rest of the paper is organized as follows. Section 2 discusses the related work. The VAEs are introduced in Section 3. We present the model architecture in Section 4. Experimental results and analyses are reported in Section 5 and Section 6. The conclusion is drawn in Section 7.

2. Related Work

2.1. Text-to-Speech Models

The goal of text-to-speech (TTS) synthesis is to convert an input text sequence into an intelligible and natural-sounding speech utterance. Most previous work divides the task

into two steps. The first step is text-to-acoustic (e.g. mel-spectrograms) modeling. Tacotron 1 & 2 (Wang et al., 2017; Shen et al., 2018), Deep Voice 2 & 3 (Gibiansky et al., 2017; Ping et al., 2018b), TransformerTTS (Li et al., 2019) and Flowtron (Valle et al., 2020) are AR models among the best performing TTS models. These models employ an encoder-decoder framework with attention mechanism, where the encoder convert the input text sequence to hidden representations and the decoder takes a weighted sum of the hidden representations to generate the output acoustic features frame by frame. It is challenging to learn the alignment between text sequence and acoustic features (e.g. mel-spectrograms) for TTS models. Various attention mechanisms are proposed to improve the stability and monotonicity of the alignment in AR models, such as location-sensitive attention (Chorowski et al., 2015), forward attention (Zhang et al., 2018), multi-head attention (Li et al., 2019), step-wise monotonic attention (He et al., 2019) location-relative attention (Battenberg et al., 2020). However, the low inference efficiency of AR models hinders their application in real-time services. Recently, non-AR models are proposed to synthesize the output in parallel. The key to design a non-AR acoustic model is the parallel alignment prediction. ParaNet (Peng et al., 2020) also adopts a layer-wise refined attention mechanism, where the queries are only positional encoding in the first attention layer and previous attention layer output processed by a convolution block in the following attention layers. However, attention distillation from pre-trained AR TTS model are still needed to guide the training of alignments. Fastspeech (Ren et al., 2019) also requires knowledge distillation from pre-trained AR TTS model to learn alignments, while Fastspeech 2 bypasses the requirement of teacher model through an external force aligner for duration labels (Ren et al., 2020). Glow-TTS (Kim et al., 2020) and Flow-TTS (Miao et al., 2020) are both flow-based non-AR TTS models. Glow-TTS enforces hard monotonic alignments through the properties of flows and dynamic programming. Flow-TTS adopts positional attention to learn the alignment during training and uses length predictor to predict spectrogram length during inference.

The second step is acoustic features to time-domain waveform samples modeling. WaveNet (Oord et al., 2016) is the first of these AR neural vocoders, which produced high quality audio. Since WaveNet inference is computationally challenging. Several AR models are proposed to improve the inference speed while retaining quality (Arik et al., 2017; Jin et al., 2018; Kalchbrenner et al., 2018). Non-AR vocoders have also attracted increasing research interest (Oord et al., 2018; Ping et al., 2018a; Prenger et al., 2019; Yamamoto et al., 2020), which generate high fidelity speech much faster than real-time.

Recently, end-to-end generation of audio samples from text sequence has been proposed in (Donahue et al., 2020; Ren

et al., 2020; Weiss et al., 2020). Wave-Tacotron extends Tacotron by incorporating a normalizing flow into the AR decoder loop. Both EATS (Weiss et al., 2020) and Fast-speech 2s (Ren et al., 2020) are non-AR models, where various adversarial feedbacks and auxiliary prediction losses are used respectively.

2.2. VAE-based Generative Models

VAE (Kingma & Welling, 2013; Rezende et al., 2014) is a widely used generative model. Both variational RNN (VRNN) (Chung et al., 2015) and vector quantised-VAE (VQ-VAE) (Van Den Oord et al., 2017) adopt AR structure to model the generative process of audio samples. (Child, 2020) verifies that VDVAE outperforms the AR model PixelCNN (Van den Oord et al., 2016) in log-likelihood on all natural image benchmarks, while using fewer parameters and generating samples thousands of times faster. Inspired by the success of the VDVAE architecture, we employ it for parallel speech synthesis task.

In parallel to our work, BVAE-TTS (Lee et al., 2021) has been proposed, where bidirectional hierarchical VAE architecture is also adopted for non-AR TTS. However, only latent variables from the toppest layer are used as queries and there is a gap between the attention-based mel-spectrogram generation during training and the duration-based mel-spectrogram generation during inference in BVAE-TTS. Therefore, various empirical and carefully-designed techniques are needed to bridge this gap. By employing a residual attention mechanism, our proposed model can eliminate this training and inference mismatch.

3. Variational autoencoders

VAEs consist of the following parts: a generator $p(\mathbf{x}|\mathbf{z})$, a prior $p(\mathbf{z})$ and a posterior $q(\mathbf{z}|\mathbf{x})$ approximator. Typically, the posteriors and priors in VAEs are assumed normally distributed with diagonal covariance, which allows for the Gaussian reparameterization trick to be used (Kingma & Welling, 2013). The generator $p(\mathbf{x}|\mathbf{z})$ and approximator $q(\mathbf{z}|\mathbf{x})$ are jointly trained by maximizing the evidence lower bound (ELBO):

$$\log p(\mathbf{x}) \geq \mathbb{E}_{\mathbf{z} \sim q(\mathbf{z}|\mathbf{x})} \log p(\mathbf{x}|\mathbf{z}) - \text{KL} [q(\mathbf{z}|\mathbf{x}) \| p(\mathbf{z})] \quad (1)$$

where the first term of the right hand side of this inequality can be seen as the expectation of negative reconstruction error and the second KL divergence term can be seen as a regularizer.

Hierarchical VAEs can gain better generative performance than previous VAEs where fully-factorized posteriors and priors are incorporated. One typical hierarchical VAE is introduced in (Sønderby et al., 2016), where both the prior $p(\mathbf{z})$ and posterior approximator $q(\mathbf{z}|\mathbf{x})$ are conditionally

dependent:

$$p(\mathbf{z}) = p(\mathbf{z}_0) p(\mathbf{z}_1|\mathbf{z}_0) \dots p(\mathbf{z}_N|\mathbf{z}_{<N}) \quad (2)$$

$$q(\mathbf{z}|\mathbf{x}) = q(\mathbf{z}_0|\mathbf{x}) q(\mathbf{z}_1|\mathbf{z}_0, \mathbf{x}) \dots q(\mathbf{z}_N|\mathbf{z}_{<N}, \mathbf{x}) \quad (3)$$

where N is the number of hierarchical groups. This hierarchical VAE first extracts latent variables from input data \mathbf{x} along the bottom-up path, then processes the latent variables along the top-down path to generate \mathbf{x} . The equation (1) is changed as follows:

$$\begin{aligned} \log p(\mathbf{x}) &\geq \mathbb{E}_{\mathbf{z} \sim q(\mathbf{z}|\mathbf{x})} \log p(\mathbf{x}|\mathbf{z}) - \text{KL} [q(\mathbf{z}_0|\mathbf{x}) \| p(\mathbf{z}_0)] \\ &\quad - \sum_{n=1}^N \mathbb{E}_{q(\mathbf{z}_{<n}|\mathbf{x})} [\text{KL} [q(\mathbf{z}_n|\mathbf{z}_{<n}, \mathbf{x}) \| p(\mathbf{z}_n|\mathbf{z}_{<n})]] \end{aligned} \quad (4)$$

where $q(\mathbf{z}_{<n}|\mathbf{x}) := \prod_{i=1}^{n-1} q(\mathbf{z}_i|\mathbf{z}_{<i}, \mathbf{x})$ is the approximate posterior up to the $(n-1)^{th}$ group.

4. Model Architecture

We adopt the VDVAE (Child, 2020) with a novel residual attention mechanism for non-AR TTS. The overall architecture is shown in Figure 1. Hierarchical latent variables at decreasing time scale are extracted from the input mel-spectrograms along the bottom-up path. These hierarchical latent variables are processed from top to bottom and served as queries (\mathbf{Q}). A text encoder takes phoneme sequence and optional speaker ID as input and outputs text encoding as key (\mathbf{K}) and value (\mathbf{V}). \mathbf{Q} , \mathbf{K} , \mathbf{V} and attention weight from previous attention block (\mathbf{A}_{prev}) are sent to the following residual attention module to produce a refined attention weight and context vector. The context vector is a weighted average of \mathbf{V} , and is passed to top-down block for variational inference and mel-spectrogram reconstruction along with stored hierarchical latent variables. A speaking speed predictor takes the mean-pooled latent variables of the coarsest layer as input and predicts the utterance-level average speaking speed factor to determine the number of acoustic frames at inference.

We use the β -VAE training objective and a mel-spectrogram loss inspired by (Rezende & Viola, 2018). The hierarchical VAE, speaking speed predictor, text encoder and residual attention modules are jointly trained with the following objective:

$$\mathcal{L} = \alpha \mathcal{L}_{\text{speaking_speed}} + \mathcal{L}_{\text{recon}} + \beta \mathcal{L}_{\text{KL}} \quad (5)$$

where,

$$\mathcal{L}_{\text{speaking_speed}} = \mathbb{E} \left(d - \hat{d} \right), \quad (6)$$

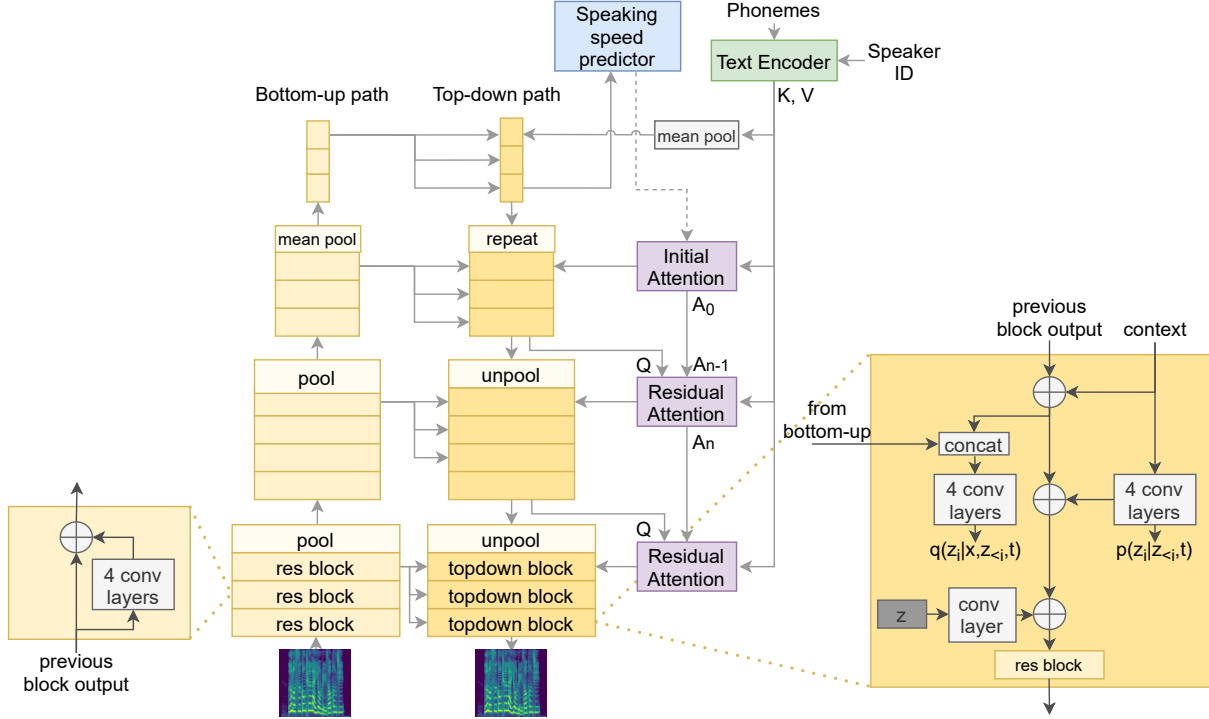


Figure 1. Overall model architecture

$$\mathcal{L}_{\text{recon}} = \frac{\|\mathbf{x} - \hat{\mathbf{x}}\|_2}{\|\mathbf{x}\|_2} + \|\log \mathbf{x} - \log \hat{\mathbf{x}}\|_1, \quad (7)$$

$$\mathcal{L}_{\text{KL}} = \text{KL} [q(\mathbf{z}_0|\mathbf{x}, \mathbf{t}) \| p(\mathbf{z}_0, \mathbf{t})] + \sum_{n=1}^N \mathbb{E}_{q(\mathbf{z}_{<n}|\mathbf{x}, \mathbf{t})} [\text{KL} [q(\mathbf{z}_n|\mathbf{x}, \mathbf{z}_{<n}, \mathbf{t}) \| p(\mathbf{z}_n|\mathbf{z}_{<n}, \mathbf{t})]], \quad (8)$$

and α, β are weights of speaking rate loss, KL loss and respectively. $\mathbf{d}, \hat{\mathbf{d}}, \mathbf{x}, \hat{\mathbf{x}}, \mathbf{t}$ and \mathbf{z} denote ground-truth speaking speed, predicted speaking speed, ground-truth mel-spectrogram magnitudes, predicted mel-spectrogram magnitudes, phoneme sequences, and latent variables respectively. We introduce detailed implementations of VDVAE, text encoder, speaking rate predictor and residual attention modules in the following subsections.

4.1. Very deep VAE

As show in the central part of Figure 1, the very deep VAE is stacked of residual block groups along the bottom-up path and topdown block groups along the top-down path. The time dimension of input mel-spectrogram is reduced at the pooling layer of each bottom-up group using average pooling. The residual block contains four convolution layers and a residual connection as shown in the left part of Figure 1. Each convolution output is preceded by the GELU nonlinearity (Hendrycks & Gimpel, 2016). The topdown block takes bottom-up output, previous topdown block output and

context vector from residual attention module as input. The previous topdown block output is unpooled at the bottom layer of each top-down group using nearest-neighbor upsampling along temporal axis, and then added to context vector as block bias for prior $p(\cdot)$ and the posterior approximator $q(\cdot)$. The bottom-up group output is concatenated with this block bias and processed by four convolution layers to predict $q(z_i|\mathbf{x}, \mathbf{z}_{<i}, \mathbf{t})$. Another path of context vector is used to predict the prior $p(z_i|\mathbf{z}_{<i}, \mathbf{t})$ through another four convolution layers. Both $q(\cdot)$ and $p(\cdot)$ are isotropic Gaussian distributions. In training stage, z is sampled from $q(\cdot)$. In inference stage, the bottom-up path is discarded and z is sampled from $p(\cdot)$. z passes a convolution layer and is added to the summation of the block bias for posterior approximator and the output of the four convolution layers, before being sent to a residual block. The residual block contains three convolution layers, one dilated convolution layer and a residual connection. z is also used as the query in the succeeding residual attention module.

Although residual connections in VDVAE are able to alleviate posterior collapse to some degree, we observe some horizontal segments in the cumulative KL curve as shown in Figure 3. This indicates that posterior collapse occurs in these layers and latent variables from these layers encode small amount of information. Therefore, we propose a detailed KL gain mechanism, inspired by (Alemi et al., 2018; Burgess et al., 2018). In hierarchical VAE, the KL

term is the accumulation of the KL terms from different hierarchical layers. We can set a reference value for each layer like the KL reference term in (Alemi et al., 2018):

$$\text{KL}_{\text{ref}} = \frac{c}{N} \sum_{i=1}^N \text{KL}_i \quad (9)$$

$$\mathcal{L}_{\text{detailed_KL_gain}} = \sum_{i=1}^N |\max(\text{KL}_i, \text{KL}_{\text{ref}}) - \text{KL}_{\text{ref}}| \quad (10)$$

where the reference KL_{ref} is the average value of KL terms from different hierarchical layers multiplied by a constant KL gain factor c ($c = 0.5$ is used in this paper). When KL_i is larger than the reference, the KL gain term is 0. When KL_i is smaller than the reference, the gain term is non-zero and the gradient of this term would enlarge the KL_i , then the ineffective latent variables would be eliminated. Therefore, the training objective of the whole model is modified as follows:

$$\mathcal{L} = \alpha \mathcal{L}_{\text{speaking_speed}} + \mathcal{L}_{\text{recon}} + \beta \mathcal{L}_{\text{KL}} + \lambda \mathcal{L}_{\text{detailed_KL_gain}} \quad (11)$$

where λ is the weight of the detailed KL gain.

4.2. Speaking speed predictor

Since number of mel-spectrogram frames to generate during inference is unknown a priori, we train an auxiliary speaking speed predictor. A two-dimensional mel-spectrogram is reduced in time-scale hierarchically along the bottom-up path and eventually to a vector \mathbf{x}_0 by a temporal global mean pooling operation; another vector \mathbf{t}_0 is obtained from the text encoder output by temporal global mean pooling. \mathbf{x}_0 and \mathbf{t}_0 are used to calculate the prior and posterior distributions for the top-most latent variables \mathbf{z}_0 . We sample a latent variable vector \mathbf{z}_0 from the latent space, which is fed into the speaking speed predictor as input. During training, \mathbf{z}_0 is sampled from the posterior $q(\mathbf{z}_0|\mathbf{x}_0, \mathbf{t}_0)$, while at inference, \mathbf{z}_0 is sampled from the prior $p(\mathbf{z}_0|\mathbf{t}_0)$.

According to the InfoGAN derivation (Chen et al., 2016), minimizing the prediction error for speaking speed from the top-most latent variables paves a way to maximizing a lower bound of their mutual information (proof in Appendix A). If the speaking speed predictor is well-trained, latent variables from the first top-down group (i.e., the top-most latent variable \mathbf{z}_0) would encode rich speaking speed information. Since latent variables (the \mathbf{z} 's) in VARA-TTS are conditionally dependent in a chain from top-to-bottom, they also contain speaking speed information, which facilitates the alignment learning at their corresponding attention modules. This alleviates the problem of inconsistency of acoustic model and a separately trained duration model. For example, the duration module of BVAE-TTS does not propagate information to the acoustic module and only uses the

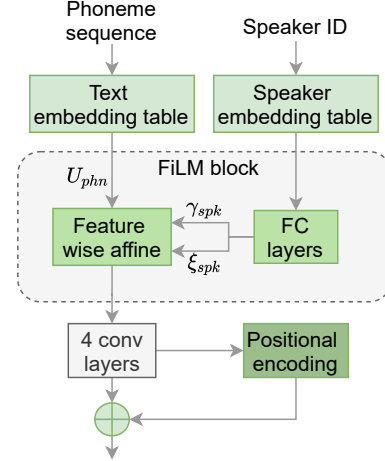


Figure 2. Network detail of text encoder

alignment obtained from the acoustic module and text encoding module as supervision. This may lead to the issue that the acoustic module is not adapted well to the duration module.

In VARA-TTS, the speaking speed predictor adopts two fully-connected (FC) layers, between which we add a ReLU activation function, a layer-normalization layer and a dropout layer in a sequence (more details are presented in Appendix D). Unlike most existing non-AR TTS models, which require token-level duration information as supervision for duration model training, we use a readily-computed speaking rate d for each training utterance as the target of the speaking speed predictor:

$$d = \text{Normalize}_{\text{min-max}}\left(\frac{T_{\text{mel}}}{L_{\text{text}}}\right) \in [0, 1], \quad (12)$$

where $\text{Normalize}_{\text{min-max}}(\cdot)$ denotes min-max normalization across the training set, T_{mel} represents the number of frames in a mel spectrogram and L_{text} is the number of tokens in a phoneme sequence. We add a sigmoid function on the speaking speed predictor output to obtain the predicted speaking rate \hat{d} . An MSE loss applied on d and \hat{d} is used as training signal for the speaking speed predictor.

4.3. Text encoder

As shown in Fig 2, phoneme sequence and speaker id are transformed to phoneme embedding and speaker embedding through two lookup tables. The feature-wise linear modulation (FiLM) (Perez et al., 2018) is used to fuse speaker embedding with phoneme embedding. Two FC layers are used to compute the scale and shift vectors from the speaker embedding vector, respectively. The feature-wise affine operation is conducted as:

$$\gamma_{\text{spk}} \times U_{\text{phn}} + \xi_{\text{spk}} \quad (13)$$

where γ_{spk} and ξ_{spk} represent the scale and shift vectors and U_{phn} represents phoneme embedding. The fused output passes four convolution layers. The convolution output and sinusoidal positional encoding (Vaswani et al., 2017) are added as text encoder output.

4.4. Residual attention

For the initial attention module in Figure 1, we simply set the attention weight matrix $\mathbf{A} \in \mathbb{R}^{T_{\text{max,red}} \times L_{\text{text}}}$ to be ‘‘nearly diagonal’’. $T_{\text{max,red}}$ is the number of feature frames before the mean pooling layer at bottom-up path. This ‘‘nearly diagonal’’ attention matrix is a good instructive bias, since the alignment between text and acoustic features are monotonic and almost diagonal. Inspired by (Tachibana et al., 2018), we set the attention weight matrix as follows:

$$S_l = \exp \left[-(t/T_{\text{max,red}} - l/L_{\text{text}})/2g^2 \right] \quad (14)$$

$$A_{tl} = S_{tl} / \sum_v S_{tlv} \quad (15)$$

where, l is text position index and t is mel-spectrogram position index. In this paper, we generate four attention matrices using $g \in [0.01, 0.05, 0.1, 0.2]$ and compute four context vectors by multiplying the four generated attention matrices with text encoder output respectively. Then the four context vectors are concatenated and projected to one context vector along temporal axis. During training stage, $T_{\text{max,red}}$ is obtained from the number of ground-truth mel-spectrogram frames divided by the maximum reduction factor. Maximum reduction factor is the product of the reduction factors between neighbouring residual block groups. During inference stage, it is obtained by multiplying predicted speaking speed \hat{d} to L_{text} and then being divided by the maximum reduction factor.

For the remaining residual attention modules, they take text encoder output (\mathbf{K}, \mathbf{V}), attention weight from previous attention module (\mathbf{A}_{prev}) and latent variables from previous topdown group (\mathbf{Q}) as input. Multi-head attention mechanism (Vaswani et al., 2017) is used, where \mathbf{A}_{prev} is added as an additional input:

$$\text{ResidualMultiHead}(\mathbf{Q}, \mathbf{K}, \mathbf{V}, \mathbf{A}_{\text{prev}}) = \text{Concat}(\text{head}_1, \dots, \text{head}_h) \mathbf{W}^O \quad (16)$$

where $\mathbf{Q}, \mathbf{K}, \mathbf{V}$ are matrices with dimension d_k, d_k and d_v respectively. $\text{head}_i = \text{ResidualAttention}(\mathbf{Q}\mathbf{W}_i^Q, \mathbf{K}\mathbf{W}_i^K, \mathbf{V}\mathbf{W}_i^V, \mathbf{A}_{\text{prev}})$. \mathbf{W}^O is the transformation matrix that linearly projects the concatenation of all heads output. $\mathbf{W}_i^Q, \mathbf{W}_i^K$ and \mathbf{W}_i^V are projection matrices of the i -th head. \mathbf{A}_{prev} is the averaged attention weights from previous attention heads. We use the scaled dot-product mechanism based residual attention:

$$\text{ResidualAttention}(\mathbf{Q}, \mathbf{K}, \mathbf{V}, \mathbf{A}_{\text{prev}}) = \text{Softmax} \left(\frac{\mathbf{Q}\mathbf{K}^T}{\sqrt{d_k}} + \mathbf{A}_{\text{prev}} \right) \mathbf{V} \quad (17)$$

We find that using attention weights \mathbf{A}_{prev} makes training process more stable than using before-softmax attention scores, which is used in RealFormer (He et al., 2020). The previous attention weight \mathbf{A}_{prev} is first upsampled to fit the time dimension and then processed by a convolution layer before being sent to the next layer. Different from the location sensitive attention (Chorowski et al., 2015) that only takes into account attention weight at previous decoder time step, our residual attention mechanism incorporates attention weights of all time steps from last residual attention module, which provides a global perspective of attention history.

5. Experiments

5.1. Data

We conduct both single-speaker and multi-speaker TTS experiments to evaluate the proposed VARA-TTS model. For single-speaker TTS, the LJSpeech corpus (Ito & Johnson, 2017) is used, which contains 13100 speech samples with total duration of about 24 hours. We up-sample the speech signals from 22.05 kHz to 24 kHz in sampling rate. The dataset is randomly partitioned into training, validation and testing sets according to a 12900/100/100 scheme. For multi-speaker TTS, we use an internal Mandarin Chinese multi-speaker corpus, which contains 55 hours of speech data from 7 female speakers.

In all experiments, mel-spectrograms are computed with 1024 window length and 256 frame shift. We convert text sentences into phoneme sequences with Festival for English and with an internal grapheme-to-phoneme toolkit for Chinese.

5.2. Model configurations

We compare VARA-TTS with a well-known AR TTS model, Tacotron 2 (Shen et al., 2018), and an analogous non-AR TTS model, BVAE-TTS (Lee et al., 2021), under single-speaker TTS setting. We use an open-source Tacotron 2 implementation² and the official BVAE-TTS implementation³. Some key hyperparameters in VARA-TTS are presented in Appendix C. To make the comparison fair, we use the same neural vocoder, HiFi-GAN (Kong et al., 2020) with HiFi-GAN-V1 configuration, to convert mel spectrograms into waveform for all three compared models.

We train the VARA-TTS model with a batch size of 32 with two NVIDIA V100 GPUs. And the model for evaluation are trained for 90k iterations. The Adam optimizer with $\beta_1 = 0.9, \beta_2 = 0.999$ is adopted for parameter updating, where the maximum of learning rate is $1.5e-4$ and scheduled

²<https://github.com/NVIDIA/tacotron2>

³<https://github.com/LEEYOONHYUNG/BVAE-TTS>

in the same manner as in (Vaswani et al., 2017) with 10k steps to warm-up.

6. Results and Analysis

6.1. Speech quality

Mean opinion score (MOS) test is conducted to evaluate the speech naturalness. We invite 10 raters to take the MOS test, where participants are asked to give a score from 1 to 5 (least natural to most natural) with 0.5 point increments to each stimuli presented. The sentences for evaluation are sampled from LibriTTS (Zen et al., 2019) test set. The MOS test results are presented in Table 1. We can see that our proposed VARA-TTS obtains higher MOS score than BVAE-TTS, while is inferior to Tacotron 2 in naturalness. We also conduct a MOS test for a multi-speaker VARA-TTS trained with the multi-speaker Mandarin corpus. The MOS result is 4.49 ± 0.11 . We can see that the MOS score on multi-speaker Mandarin corpus is much higher than the result on LJSpeech. One possible reason may be that the multi-speaker Mandarin corpus is of higher quality and contains larger amount of data. VARA-TTS is data-hungry and tends to over-fit on LJSpeech. Audio samples can be found online⁴.

6.2. Inference speed

Benefiting from its non-AR structure, VARA-TTS enjoys fast inference speed. We use the test set to compare the inference speed of the three compared models. Average inference speed of the three compared models obtained from 10 different runs on one NVIDIA GeForce RTX 2080 Ti GPU is presented in Table 1. We can see that inference speed of our VARA-TTS is 16x faster than that of Tacotron 2, and at the same scale as that of BVAE-TTS.

6.3. Alignment refinement process

Figure B.1 in Appendix B shows an example of the alignment refinement process for an utterance by the well-trained multi-speaker VARA-TTS model. In the figure, the bottom row shows the initial alignments, which show diagonal patterns generated by rule. In the second row, a blur alignment is generated. The blurriness indicates that the alignment is not reliable. However, VARA-TTS learns to refine the coarse alignment and obtain clearer alignments during the succeeding hierarchies, as can be seen from the upper plots in Figure B.1. Moreover, we observe that the alignment refinement process varies with the β value used. For $\beta = 1.0$, the alignments disperse in upper layers, and remain clear for $\beta = 1.8$. This indicates that hierarchical latent variables from the same layers encode different information when

⁴<https://vara-tts.github.io/VARA-TTS/>

Table 1. MOS with 95% confidence and inference speed results.

Model	MOS	Inference speed (ms)
Tacotron 2	4.11 ± 0.22	526.52
BVAE-TTS	3.33 ± 0.18	18.06
VARA-TTS	3.88 ± 0.20	32.01

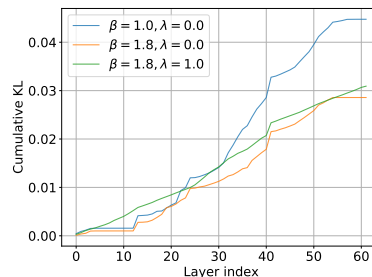


Figure 3. Cumulative KL for different β and λ . The y-axis is the cumulative KL value per data point by layers and the x-axis is the layer index. Flat horizontal line segment indicates that posterior collapse occurs in the corresponding layers.

trained with different values of β .

6.4. Ablation studies

To show the effectiveness of model design in VARA-TTS, we conduct the following ablation studies: (i) Train without detailed KL gain; (ii) Use different values of β in Equation 11 during training; (iii) Separately train the speaking speed predictor.

Detailed KL gain. Figure 3 shows the cumulative KL divergence curves with different values of β and λ . We can see that there are some horizontal segments in the cumulative KL divergence curve when $\lambda = 0$. This indicates KL values are 0 and posterior collapse occurs in the corresponding layers. When detailed KL gain is applied ($\lambda = 1.0$), the cumulative KL increases smoothly with the layer index and contains no horizontal segments. The KL value of $\lambda = 1.0$ is larger than that of $\lambda = 0$ in Figure 3. This is because detailed KL gain mechanism enlarges the hierarchical KL values smaller than KL_{ref} , which can be compensated by a larger β . We also observe that when trained with detailed KL gain, VARA-TTS can learn clearer alignments in coarse hierarchical layer as shown in Appendix B. This indicates that posterior collapse does not happen in these layers and the latent variables encode meaningful information.

Different values of β . At training, the queries are sampled from posterior, but sampled from prior at inference. Smaller KL value indicates smaller gap between prior and posterior for VDVAE. The smaller the gap between prior and posterior, the more reliable the queries can be at inference. The hyperparameter β in Equation 11 adjusts the relative weight between the reconstruction error and KL term. The

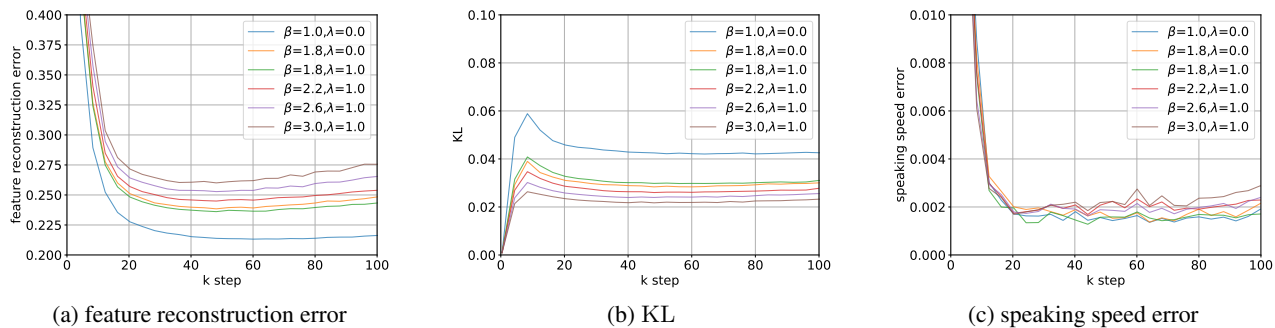


Figure 4. The feature reconstruction error, KL, and speaking speed error training curves on validation set with different values of β and λ . The x-axis is training step in the unit of thousand and the y-axis is the corresponding value of feature reconstruction error, KL, and speaking speed error.

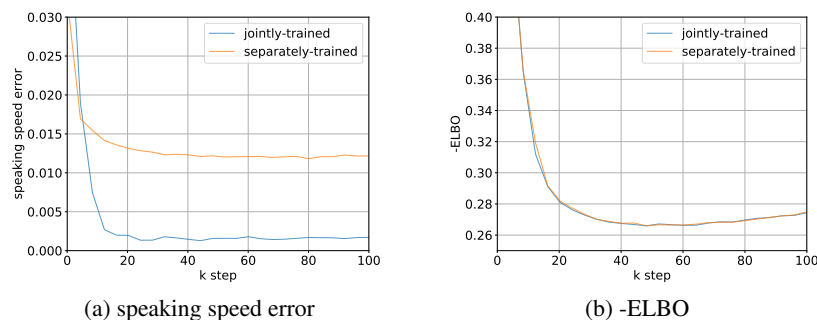


Figure 5. Speaking speed error and -ELBO for models trained with a joint speaking speed predictor and a separate one

curves of feature reconstruction error and KL value with different values of β and λ on validation set are shown in Figure 4 (a) and (b) respectively. As can be seen, enlarging β results in larger feature reconstruction error and smaller KL value. However, we find that small changes in feature reconstruction error do not influence perpetual result a lot. Figure 4 (c) shows the speaking speed error on validation set. We can see that different values of β have little effect on speaking speed error. We use $\beta = 1.8$ and $\lambda = 1.0$ for model evaluation.

Joint speaking speed modeling. The separate speaking speed predictor has the same structure as the joint one, except that its input is the mean-pooled text embedding and detached from the computational graph by a stop gradient operation. The stop gradient operation is also applied in BVAE-TTS and GLOW-TTS to avoid affecting the training objective. As show in Figure 5, the joint training strategy obtains similar ELBO as the separate training counterpart, but attains much smaller speaking speed error on validation set. This validates the effectiveness of joint training the speaking speed predictor and the whole model.

7. Conclusion

In this work, we propose a novel non-AR end-to-end TTS model, VARA-TTS, generating mel-spectrogram from text with VDVAE and residual attention mechanism. The hierarchical latent variables from VDVAE are used as queries for the residual attention module. The residual attention module is able to generate the textual-to-acoustic alignment in a layer-by-layer coarse-to-fine manner. Experimental results show that VARA-TTS attains better perceptual results than BVAE-TTS at a similar inference speed, and is 16x speed-up for inference over Tacotron 2 with slightly inferior performance in naturalness. We also demonstrate its extensibility to a multi-speaker setting.

VARA-TTS should be easily extended to text-to-waveform by adding more layers. However, we find that it is hard to optimize in our preliminary experiments. The model is able to learn clear alignment between text and waveform, but it can not generate intelligible waveform. This is consistent with the results reported in (Child, 2020) where VDVAE can not generate consistent and sharp 1024×1024 images. We propose detailed KL gain for VDVAE, which can avoid non-informative hierarchical latent variables. It is interesting to analyze it theoretically and we leave this for the future work.

References

- Alemi, A. A., Poole, B., Fischer, I., Dillon, J. V., Saurous, R. A., and Murphy, K. Fixing a broken ELBO. In Dy, J. G. and Krause, A. (eds.), *Proceedings of the 35th International Conference on Machine Learning, ICML 2018, Stockholmsmässan, Stockholm, Sweden, July 10-15, 2018*, volume 80 of *Proceedings of Machine Learning Research*, pp. 159–168. PMLR, 2018.
- Arik, S. O., Chrzanowski, M., Coates, A., Diamos, G., Gibiansky, A., Kang, Y., Li, X., Miller, J., Ng, A., Raiman, J., et al. Deep voice: Real-time neural text-to-speech. *arXiv preprint arXiv:1702.07825*, 2017.
- Battenberg, E., Skerry-Ryan, R., Mariooryad, S., Stanton, D., Kao, D., Shannon, M., and Bagby, T. Location-relative attention mechanisms for robust long-form speech synthesis. In *ICASSP 2020-2020 IEEE International Conference on Acoustics, Speech and Signal Processing (ICASSP)*, pp. 6194–6198. IEEE, 2020.
- Burgess, C. P., Higgins, I., Pal, A., Matthey, L., Watters, N., Desjardins, G., and Lerchner, A. Understanding disentangling in β -vae. *CoRR*, abs/1804.03599, 2018.
- Chen, X., Duan, Y., Houthoofd, R., Schulman, J., Sutskever, I., and Abbeel, P. Infogan: Interpretable representation learning by information maximizing generative adversarial nets. In *NIPS*, 2016.
- Child, R. Very deep vaes generalize autoregressive models and can outperform them on images. *arXiv preprint arXiv:2011.10650*, 2020.
- Chorowski, J. K., Bahdanau, D., Serdyuk, D., Cho, K., and Bengio, Y. Attention-based models for speech recognition. *Advances in neural information processing systems*, 28:577–585, 2015.
- Chung, J., Kastner, K., Dinh, L., Goel, K., Courville, A. C., and Bengio, Y. A recurrent latent variable model for sequential data. *Advances in neural information processing systems*, 28:2980–2988, 2015.
- Donahue, J., Dieleman, S., Bifinkowski, M., Elsen, E., and Simonyan, K. End-to-end adversarial text-to-speech. *arXiv preprint arXiv:2006.03575*, 2020.
- Gibiansky, A., Arik, S., Diamos, G., Miller, J., Peng, K., Ping, W., Raiman, J., and Zhou, Y. Deep voice 2: Multi-speaker neural text-to-speech. In *Advances in neural information processing systems*, pp. 2962–2970, 2017.
- He, M., Deng, Y., and He, L. Robust sequence-to-sequence acoustic modeling with stepwise monotonic attention for neural tts. *Proc. Interspeech 2019*, pp. 1293–1297, 2019.
- He, R., Ravula, A., Kanagal, B., and Ainslie, J. Real-former: Transformer likes residual attention. *CoRR*, abs/2012.11747, 2020.
- Hendrycks, D. and Gimpel, K. Gaussian error linear units (gelus). *arXiv preprint arXiv:1606.08415*, 2016.
- Ito, K. and Johnson, L. The lj speech dataset. <https://keithito.com/LJ-Speech-Dataset/>, 2017.
- Jin, Z., Finkelstein, A., Mysore, G. J., and Lu, J. Fftnet: A real-time speaker-dependent neural vocoder. In *2018 IEEE International Conference on Acoustics, Speech and Signal Processing (ICASSP)*, pp. 2251–2255. IEEE, 2018.
- Kalchbrenner, N., Elsen, E., Simonyan, K., Noury, S., Casagrande, N., Lockhart, E., Stimberg, F., Oord, A. v. d., Dieleman, S., and Kavukcuoglu, K. Efficient neural audio synthesis. *arXiv preprint arXiv:1802.08435*, 2018.
- Kim, J., Kim, S., Kong, J., and Yoon, S. Glow-tts: A generative flow for text-to-speech via monotonic alignment search. *arXiv preprint arXiv:2005.11129*, 2020.
- Kingma, D. P. and Welling, M. Auto-encoding variational bayes. *arXiv preprint arXiv:1312.6114*, 2013.
- Kong, J., Kim, J., and Bae, J. Hifi-gan: Generative adversarial networks for efficient and high fidelity speech synthesis. In Larochelle, H., Ranzato, M., Hadsell, R., Balcan, M., and Lin, H. (eds.), *Advances in Neural Information Processing Systems 33: Annual Conference on Neural Information Processing Systems 2020, NeurIPS 2020, December 6-12, 2020, virtual*, 2020.
- Lee, Y., Shin, J., and Jung, K. Bidirectional variational inference for non-autoregressive text-to-speech. In *International Conference on Learning Representations*, 2021. URL <https://openreview.net/forum?id=o3iritJHLf0>.
- Li, N., Liu, S., Liu, Y., Zhao, S., and Liu, M. Neural speech synthesis with transformer network. In *Proceedings of the AAAI Conference on Artificial Intelligence*, volume 33, pp. 6706–6713, 2019.
- Miao, C., Liang, S., Chen, M., Ma, J., Wang, S., and Xiao, J. Flow-tts: A non-autoregressive network for text to speech based on flow. In *ICASSP 2020-2020 IEEE International Conference on Acoustics, Speech and Signal Processing (ICASSP)*, pp. 7209–7213. IEEE, 2020.
- Oord, A., Li, Y., Babuschkin, I., Simonyan, K., Vinyals, O., Kavukcuoglu, K., Driessche, G., Lockhart, E., Cobo, L., Stimberg, F., et al. Parallel wavenet: Fast high-fidelity speech synthesis. In *International conference on machine learning*, pp. 3918–3926. PMLR, 2018.

- Oord, A. v. d., Dieleman, S., Zen, H., Simonyan, K., Vinyals, O., Graves, A., Kalchbrenner, N., Senior, A., and Kavukcuoglu, K. Wavenet: A generative model for raw audio. *arXiv preprint arXiv:1609.03499*, 2016.
- Peng, K., Ping, W., Song, Z., and Zhao, K. Non-autoregressive neural text-to-speech. In *International Conference on Machine Learning*, pp. 7586–7598. PMLR, 2020.
- Perez, E., Strub, F., De Vries, H., Dumoulin, V., and Courville, A. Film: Visual reasoning with a general conditioning layer. In *Proceedings of the AAAI Conference on Artificial Intelligence*, volume 32, 2018.
- Ping, W., Peng, K., and Chen, J. Clarinet: Parallel wave generation in end-to-end text-to-speech. In *International Conference on Learning Representations*, 2018a.
- Ping, W., Peng, K., Gibiansky, A., Arik, S. O., Kannan, A., Narang, S., Raiman, J., and Miller, J. Deep voice 3: 2000-speaker neural text-to-speech. *Proc. ICLR*, pp. 214–217, 2018b.
- Prenger, R., Valle, R., and Catanzaro, B. Waveglow: A flow-based generative network for speech synthesis. In *ICASSP 2019-2019 IEEE International Conference on Acoustics, Speech and Signal Processing (ICASSP)*, pp. 3617–3621. IEEE, 2019.
- Ren, Y., Ruan, Y., Tan, X., Qin, T., Zhao, S., Zhao, Z., and Liu, T.-Y. FastSpeech: Fast, robust and controllable text to speech. *Advances in Neural Information Processing Systems*, 32:3171–3180, 2019.
- Ren, Y., Hu, C., Qin, T., Zhao, S., Zhao, Z., and Liu, T.-Y. FastSpeech 2: Fast and high-quality end-to-end text-to-speech. *arXiv preprint arXiv:2006.04558*, 2020.
- Rezende, D. J. and Viola, F. Taming vaes. *CoRR*, abs/1810.00597, 2018.
- Rezende, D. J., Mohamed, S., and Wierstra, D. Stochastic backpropagation and approximate inference in deep generative models. In *International Conference on Machine Learning*, pp. 1278–1286, 2014.
- Shen, J., Pang, R., Weiss, R. J., Schuster, M., Jaitly, N., Yang, Z., Chen, Z., Zhang, Y., Wang, Y., Skerry-Ryan, R., et al. Natural tts synthesis by conditioning wavenet on mel spectrogram predictions. In *2018 IEEE International Conference on Acoustics, Speech and Signal Processing (ICASSP)*, pp. 4779–4783. IEEE, 2018.
- Sønderby, C. K., Raiko, T., Maaløe, L., Sønderby, S. K., and Winther, O. Ladder variational autoencoders. In *Advances in neural information processing systems*, pp. 3738–3746, 2016.
- Tachibana, H., Uenoyama, K., and Aihara, S. Efficiently trainable text-to-speech system based on deep convolutional networks with guided attention. In *2018 IEEE International Conference on Acoustics, Speech and Signal Processing, ICASSP 2018, Calgary, AB, Canada, April 15-20, 2018*, pp. 4784–4788. IEEE, 2018.
- Valle, R., Shih, K., Prenger, R., and Catanzaro, B. Flowtron: an autoregressive flow-based generative network for text-to-speech synthesis. *arXiv preprint arXiv:2005.05957*, 2020.
- Van den Oord, A., Kalchbrenner, N., Espeholt, L., Vinyals, O., Graves, A., et al. Conditional image generation with pixelcnn decoders. *Advances in neural information processing systems*, 29:4790–4798, 2016.
- Van Den Oord, A., Vinyals, O., et al. Neural discrete representation learning. In *Advances in Neural Information Processing Systems*, pp. 6306–6315, 2017.
- Vaswani, A., Shazeer, N., Parmar, N., Uszkoreit, J., Jones, L., Gomez, A. N., Kaiser, L., and Polosukhin, I. Attention is all you need. In Guyon, I., von Luxburg, U., Bengio, S., Wallach, H. M., Fergus, R., Vishwanathan, S. V. N., and Garnett, R. (eds.), *Advances in Neural Information Processing Systems 30: Annual Conference on Neural Information Processing Systems 2017, December 4-9, 2017, Long Beach, CA, USA*, pp. 5998–6008, 2017.
- Wang, Y., Skerry-Ryan, R., Stanton, D., Wu, Y., Weiss, R. J., Jaitly, N., Yang, Z., Xiao, Y., Chen, Z., Bengio, S., et al. Tacotron: Towards end-to-end speech synthesis. *Proc. Interspeech 2017*, pp. 4006–4010, 2017.
- Weiss, R. J., Skerry-Ryan, R., Battenberg, E., Miao, Y., and Kingma, D. P. Wave-tacotron: Spectrogram-free end-to-end text-to-speech synthesis. *arXiv preprint arXiv:2011.03568*, 2020.
- Yamamoto, R., Song, E., and Kim, J.-M. Parallel wavegan: A fast waveform generation model based on generative adversarial networks with multi-resolution spectrogram. In *ICASSP 2020-2020 IEEE International Conference on Acoustics, Speech and Signal Processing (ICASSP)*, pp. 6199–6203. IEEE, 2020.
- Zen, H., Dang, V., Clark, R., Zhang, Y., Weiss, R. J., Jia, Y., Chen, Z., and Wu, Y. Libritts: A corpus derived from librispeech for text-to-speech. *CoRR*, abs/1904.02882, 2019.
- Zhang, J.-X., Ling, Z.-H., and Dai, L.-R. Forward attention in sequence-to-sequence acoustic modeling for speech synthesis. In *2018 IEEE International Conference on Acoustics, Speech and Signal Processing (ICASSP)*, pp. 4789–4793. IEEE, 2018.

Supplement Materials

A. Auxiliary speaking speed predictor proof

Minimizing the prediction error for speaking speed d from the top-most latent variables \mathbf{z}_0 paves the way to maximizing a lower bound of their mutual information.

Proof

$$\begin{aligned}
 I(\mathbf{z}_0; d) &= -\mathbb{H}(d|\mathbf{z}_0) + \mathbb{H}(d) \\
 &= \mathbb{E}_{\mathbf{z}_0 \sim p(\mathbf{z}_0)} [\mathbb{E}_{d \sim p(d|\mathbf{z}_0)} [\log p(d|\mathbf{z}_0)]] + \mathbb{H}(d) \\
 &= \mathbb{E}_{\mathbf{z}_0 \sim p(\mathbf{z}_0)} [D_{\text{KL}}(p(d|\mathbf{z}_0) || q(d|\mathbf{z}_0)) + \mathbb{E}_{d \sim p(d|\mathbf{z}_0)} [\log q(d|\mathbf{z}_0)]] + \mathbb{H}(d) \\
 &\geq \mathbb{E}_{\mathbf{z}_0 \sim p(\mathbf{z}_0)} [\mathbb{E}_{d \sim p(s|\mathbf{z}_0)} [\log q(d|\mathbf{z}_0)]] + \mathbb{H}(d) \\
 &= \mathbb{E}_{d \sim p(d)} [\mathbb{E}_{\mathbf{z}_0 \sim p(\mathbf{z}_0|d)} [\log q(d|\mathbf{z}_0)]] + \mathbb{H}(d)
 \end{aligned}$$

$I(\mathbf{z}_0; d)$ is the mutual information between \mathbf{z}_0 and d . $\mathbb{H}(d|\mathbf{z}_0)$ is the conditional entropy of d given \mathbf{z}_0 and $\mathbb{H}(d)$ is the entropy of d . Each piece of datum (\mathbf{x} and \mathbf{t}) has its corresponding d . $p(\mathbf{z}_0)$ is the prior distribution of \mathbf{z}_0 given \mathbf{t} , which omitted for conciseness. $p(d)$ is the prior of d . It is not actually sampled. d is sampled when a piece of datum is sampled. $q(d|\mathbf{z}_0)$ is the output distribution of an auxiliary speaking speed predictor. $p(\mathbf{z}_0|d)$ is actually the posterior of \mathbf{z}_0 given \mathbf{x} and \mathbf{t} .

B. Alignments for different values of β and γ .

Figure B.1 shows alignments for different values of β and γ .

C. Detailed model configuration

Details of some key hyperparameters in VARA-TTS are listed in Table 1. For the remaining model configuration, please refer to the source code accompanied with this manuscript.

D. Speaking speed predictor network structure

Network structure of the speaking speed predictor used in VARA-TTS is illustrated in Figure D.1.

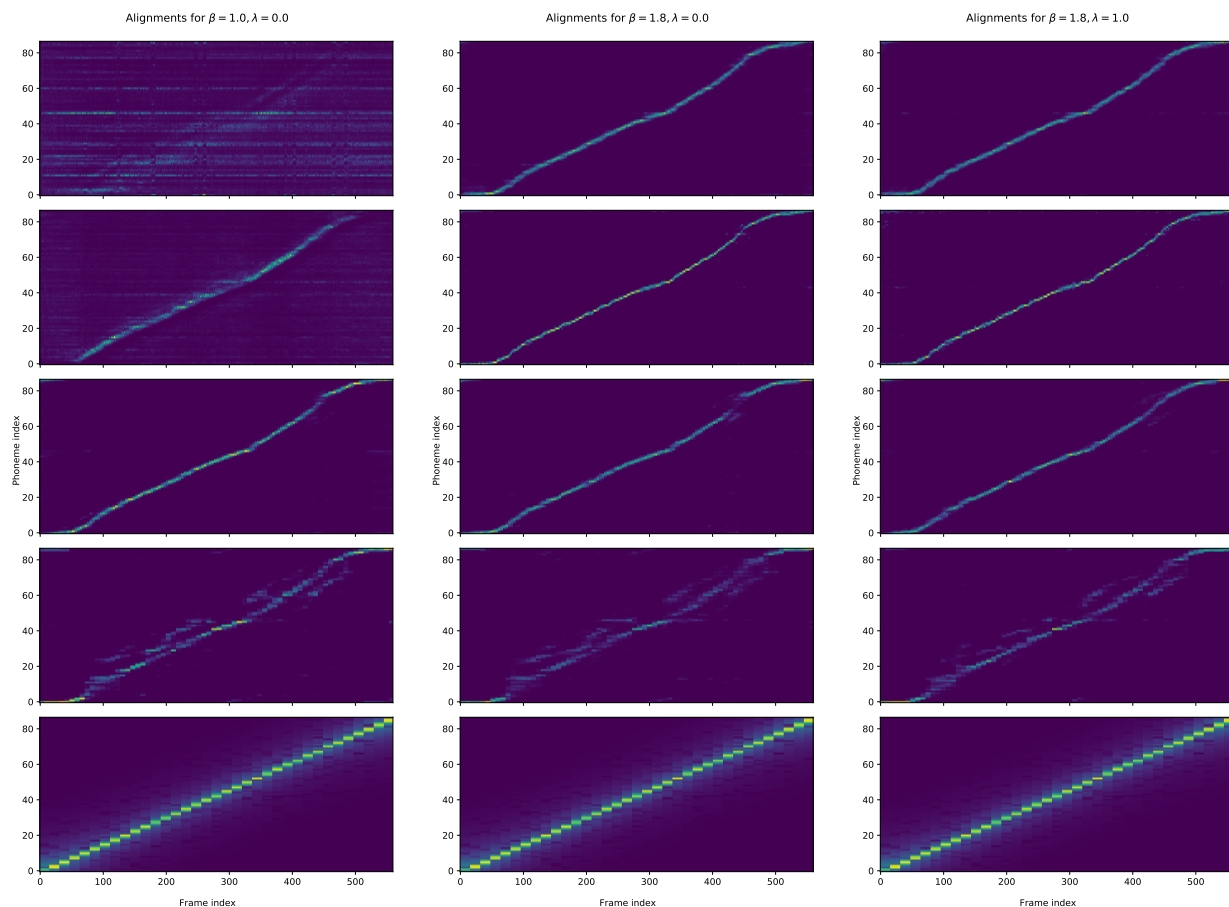


Figure B.1. Alignments for different values of β and λ . All the alignments are interpolated to the highest temporal resolution. The figures from bottom row to top row correspond to coarse to fine hierarchical layers. The alignments on the bottom row are diagonal alignments generated according to lengths of text and acoustic features. The following alignments are generated by residual attention mechanism. The alignments become clearer at finer hierarchical layers when $\beta = 1.8$. However, when $\beta = 1.0$, the alignments at finer hierarchical layers become blurry. When $\lambda = 1.0$, the alignments at coarse layers is clearer than those when $\lambda = 0$.

Table 1. Hyperparameters in VARA-TTS.

Hyperparameter name	VARA-TTS(EN)	VARA-TTS(ZH)
Number of mel banks in mel spectrogram	80	80
Mel spectrogram pre-conv layer	Conv1D with k=11 and c=384	Conv1D with k=11 and c=512
Number of phoneme tokens	55	148
Text embedding dimension	384	384
Total number of bottom-up stacks	6	7
Number of res blocks in each bottom-up stack	4/6/8/12/9/5	6/12/16/10/8/8/5
Temporal reduction rate in each bottom-up stack	repeat/2/2/2/2/1	repeat/2/2/2/2/1
Bottom-up residual block conv dimensions	384/96/96/384	512/128/128/512
Number of heads in multihead attention module	8	8
Attention dimension	384	384
Latent variable dimension	16	16
Text encoder conv dimensions	384/96/96/384	384/96/96/384
Number of speakers	1	7
Speaker embedding dimension	-	384

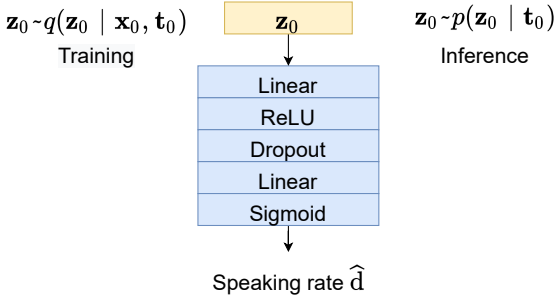


Figure D.1. Network detail of speaking speed predictor in VARA-TTS